Solid State Ionics 180 (2009) 13–17

Contents lists available at ScienceDirect

Solid State Ionics

journal homepage: www.elsevier.com/locate/ssi

Atomistic calculation of association energy in doped ceria

Xi Wei [a], Wei Pan [a,*], Laifei Cheng [b], Bin Li [a]

[a] State Key Laboratory of New Ceramics and Fine Processing, Department of Materials Science and Engineering, Tsinghua University, Beijing, 100084, PR China
[b] National Key Laboratory of Thermostructure Composite Materials, College of Materials Science, Northwestern Polytechnical University, Xi'an 710072, PR China

ARTICLE INFO

Article history:
Received 16 May 2008
Received in revised form 16 October 2008
Accepted 20 October 2008

Keywords:
Doped CeO_2
Atomistic simulation
Association energy
Defect associate
Ionic conductivity

ABSTRACT

Atomistic simulation based on energy minimization techniques was carried out to study the association energies of more than 300 defect structures of ceria doped with Lu_2O_3, Yb_2O_3, Er_2O_3, Y_2O_3, Gd_2O_3, Eu_2O_3, Sm_2O_3, Nd_2O_3 and La_2O_3. The calculation ensemble includes all the possible defect structures in 6.25 mol% doped ceria. It is revealed that a clear preference for vacancy–dopant association occurs energetically for small dopant cations and vacancy–Ce^{4+} association for large dopant cations, with the crossover at Gd^{3+}. The defect structures with the maximum association effect for different trivalent cations were determined. For Gd^{3+} doped ceria which presents the lowest association effect in the trivalent doped ceria, the association energies of four different defect structures are extremely close, which agrees well with a recent EXAFS investigation, that is, Gd^{3+} is distributed randomly in the ceria lattice. This work provides insight for the understanding of ionic conductivity in doped ceria.

1. Introduction

Ceria doped with trivalent oxides, especially the lanthanide oxides, is widely regarded as an interesting candidate for electrolyte membranes in oxygen sensors, oxygen pumps and solid oxide fuel cells (SOFC) which are expected to become a promising high-efficiency electrical power generator that enables clean energy production and support sustainable development [1–4]. One of the most prominent properties of doped ceria is its high ionic conductivity arising from charge compensating oxygen vacancies related to aliovalent cation additions. The ionic conductivity (σ) of doped ceria can be represented by the conventional *Arrhenius* relationship:

$$\sigma T = \sigma_0 \exp\left(-\frac{E_a}{k_B T}\right) \quad (1)$$

where T is the absolute temperature, k_B is the Boltzman constant, E_a is the activation energy for oxygen vacancy diffusion, σ_0 is the apparent pre-exponential factor which can be expressed as [4]:

$$\sigma_0 = \left(\frac{q_v^2}{k}\right) a^2 \nu_0 C_v \exp\left(\frac{\Delta S_m}{k}\right) \quad (2)$$

where q_v is the electronic charge of an oxygen vacancy, a is the jump distance of a vacancy, ν_0 is an appropriate lattice vibration frequency, C_v is the number of anion vacancies per unit volume and ΔS_m is the activation entropy of diffusion. Eq. (1) implies that a lower E_a leads to a higher ionic conductivity. It would be reasonable to assume that the vacancies induced by doping with aliovalent cations are not free but bound to dopant cations to form defect associates (or defect clusters) [5,6]. As the thermal dissociation of defect associates requires a supplementary energy in addition to the energy for migration of free oxygen vacancies, the activation energy for oxygen diffusion thus consists of association energy and migration energy [7,8]. Hence, for the doped ceria, E_a can be divided into association energy (or binding energy) E_{ass} and migration energy E_m. At a sufficiently high temperature, most vacancies will be dissociated, therefore the major defects are $V_O^{\cdot\cdot}$ and M_{Ce}' and the defect association is negligible. At a rather low temperature, the defect association becomes perceptible. For current SOFC research, an important focus is to reduce cost by lowering the operating temperature below 500 °C, i.e., conditions under which the defect association effect must be taken into account. Therefore, a deep understanding of association energy in doped ceria is needed and a clear comprehension of the physics behind the association energy related to ionic conductivity would be very helpful for further application of doped ceria in SOFC. Besides elaborate experimental work, atomistic simulation and theoretic calculation have been regarded as realistic and powerful tools to thoroughly understand the defect properties on an atomic level. Theoretic studies based on both semi-empirical atomistic simulation and first principle calculations were carried out to investigate the atom-level defect properties of doped ceria [9–14]. For example, Minervini et al. [10] used atomistic simulations to study the binding energy of a series of trivalent cation doped ceria. It was found that small dopant ions prefer to occupy first neighbour sites, large dopant ions prefer second neighbour sites, and the crossover occurs at approximately Gd, which also exhibits the smallest binding energy. Ball et al. [12] used atomic

* Corresponding author.
E-mail addresses: libra_wei@163.com (X. Wei), panw@mail.tsinghua.edu.cn (W. Pan).

0167-2738/$ – see front matter © 2008 Elsevier B.V. All rights reserved.
doi:10.1016/j.ssi.2008.10.019

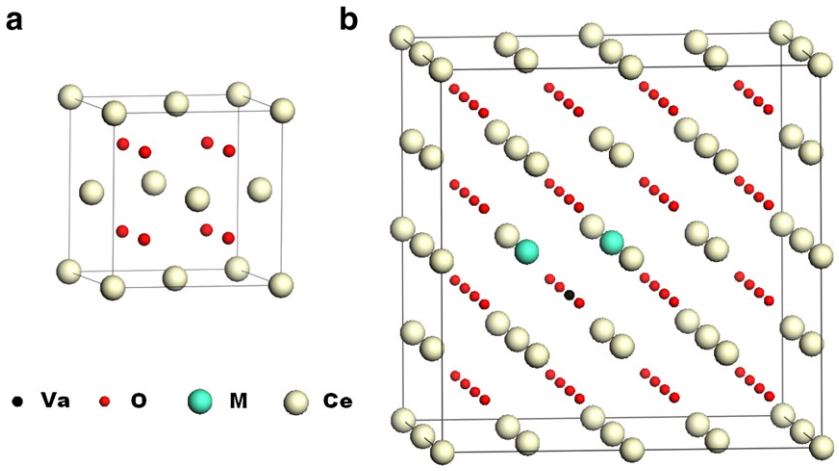

Fig. 1. The fluorite structure of ceria and the 2×2×2 supercell used to study its defect properties. a) unit cell of ceria (8 anion sites and 4 cation sites); b) one of the defect structures (1_1_1) within 2×2×2 ceria supercell (63 O^{2-} sites, 1 vacancy site, 30 Ce^{4+} sites and 2 M^{3+} sites). M represents the trivalent dopant cation. The corresponding concentration for dopant cation is 6.25 mol%.

scale computer simulations to calculate the association energy of Gd_2O_3 doped ceria. The binding energies of the defect clusters were accurately described by a model in which the total binding energy is deconvoluted into its constituent pair terms. But it was suggested that the approach will be useful only for describing fluorite systems with low dopant concentrations (i.e. <1%). First principles density functional theory (DFT) calculations have been used to study migration energy of Y, La, and Sm doped ceria in [13] and to study the activation energy in a series of lanthanide cation doped ceria in [14]. A general deficiency of the previous works is that only limited local atomic configurations are considered and no study of doped ceria is on the basis of a complete description of the local atomic configuration space.

In this study, we make efforts for the first time to calculate the association energies of all the possible defect structures within a 2×2×2 CeO_2 supercell, derived from the ideal fluorite structure (Fig. 1). We replace two Ce ions with two trivalent dopant cations and remove one O ion from the oxygen sublattice. The corresponding molar concentration of dopant cation is 6.25 mol%. We first substituted a dopant cation named M1 for the Ce^{4+} in the center of the 2×2×2 CeO_2 supercell. Following this, another dopant cation named M2 was introduced into the supercell. In the cation sublattice, there are five cation coordination shells around M1. Finally, an oxygen vacancy was introduced into the supercell. In the anion sublattice where the vacancy is located, there are four coordination shells around M1 and eight possible distances for M2. All the possible defect structures are displayed in Table 1. 35 different defect structures were considered for each type of dopant cation. A calculation ensemble of more than 300 defect structures of ceria doped with Lu_2O_3, Yb_2O_3, Er_2O_3, Y_2O_3, Gd_2O_3, Eu_2O_3, Sm_2O_3, Nd_2O_3 and La_2O_3 was carried out using atomistic simulations based on energy minimization techniques.

Table 1
All defect structures in 2×2×2 CeO_2 supercell with two trivalent cations and a vacancy

No.	M1*–M2	M1-vacancy	M2-vacancy	Defect structure symbols
1	1NN	1NN	1NN	1_1_1
2	1NN	1NN	2NN	1_1_2
3	1NN	1NN	3NN	1_1_3
4	1NN	2NN	2NN	1_2_2
5	1NN	2NN	3NN	1_2_3
6	1NN	2NN	4NN	1_2_4
7	1NN	2NN	5NN	1_2_5
8	1NN	3NN	3NN	1_3_3
9	1NN	3NN	4NN	1_3_4
10	1NN	3NN	5NN	1_3_5
11	1NN	3NN	6NN	1_3_6
12	1NN	3NN	7NN	1_3_7
13	1NN	4NN	5NN	1_4_5
14	1NN	4NN	8NN	1_4_8
15	2NN	1NN	2NN	2_1_2
16	2NN	2NN	3NN	2_2_3
17	2NN	3NN	4NN	2_3_4
18	3NN	1NN	2NN	3_1_2
19	3NN	1NN	3NN	3_1_3
20	3NN	1NN	4NN	3_1_4
21	3NN	2NN	2NN	3_2_2
22	3NN	2NN	3NN	3_2_3
23	3NN	2NN	5NN	3_2_5
24	3NN	2NN	6NN	3_2_6
25	3NN	3NN	4NN	3_3_4
26	3NN	3NN	5NN	3_3_5
27	3NN	3NN	7NN	3_3_7
28	3NN	4NN	4NN	3_4_4
29	3NN	4NN	7NN	3_4_7
30	4NN	1NN	3NN	4_1_3
31	4NN	2NN	2NN	4_2_2
32	4NN	2NN	4NN	4_2_4
33	4NN	3NN	3NN	4_3_3
34	5NN	1NN	4NN	5_1_4
35	5NN	2NN	3NN	5_2_3

*M1 and M2 represent the two dopant cations. The 1NN, 2NN, etc., represent the first nearest neighbor, second nearest neighbor, etc. In the defect structure symbols, the first number represents the separation of M1–M2, and the other two numbers represent the separations of M1-vacancy and M2-vacancy. The M1 and M2 refer to the same dopant cations in this article.

2. Methods

Atomistic simulation of ionic materials is a well-established computational tool for which comprehensive accounts can be found [15,16]. For this reason, only a concise description will be given here. The constitute ions of the doped ceria are treated as classical charged particles interacting with each other through long range Coulombic forces which are summed using Ewald's method [17] and also through short range forces that are modeled using the parameterized pair potential

$$\phi_{ij} = A\exp\left(\frac{-r_{ij}}{\rho}\right) - \frac{C}{r_{ij}^6} \tag{3}$$

where the interaction potential ϕ_{ij} involving ions i and j at distance r_{ij} depends on three adjustable empirical parameters A, ρ, and C. The short-range term accounts for the electron–cloud overlap and dispersion interactions, which are negligible beyond a few lattice spacings. Thus, a potential cutoff of 20 Å was adopted in all calculations. The potential parameters between cation and oxygen ion were presented in Table 2.

Table 2
Short-range potential parameters used in calculations [18–20]

Species	A (eV)	ρ (Å)	C (eV·Å^6)
O^{2-}–O^{2-}	9547.96	0.2192	32.00
Lu^{3+}–O^{2-}	1618.80	0.3385	19.27
Yb^{3+}–O^{2-}	1649.80	0.3386	16.57
Er^{3+}–O^{2-}	1739.91	0.3389	17.55
Y^{3+}–O^{2-}	1766.40	0.3385	19.43
Gd^{3+}–O^{2-}	1885.75	0.3399	20.34
Eu^{3+}–O^{2-}	1925.71	0.3403	20.59
Sm^{3+}–O^{2-}	1944.44	0.3414	21.49
Nd^{3+}–O^{2-}	1995.20	0.3430	22.59
La^{3+}–O^{2-}	2088.79	0.3460	23.25
Ce^{4+}–O^{2-}	1809.68	0.3547	20.40

In all calculations, ionic polarizability was taken into account for the O^{2-} and Ce^{4+} through the shell model [21], in which an ion is represented as a massive core connected to a massless shell by an isotropic harmonic spring force constant k (see Table 3). Displacement of the shell relative to the core gives a good description of electronic polarization. The dopant cations were assumed to be unpolarizable. Indeed, atomistic simulations of similar systems indicate that cation polarizability has little influence on the results [10,11].

Defects were treated with a two-region strategy in which the crystal is partitioned into two spherical regions. The inner region I is centered on the defect and the ions in region I are relaxed individually under the defect perturbation. Interactions in region I are calculated explicitly so that the response of the lattice to the defect is modeled by relaxing the positions of all ions to zero force using a Broyden–Fletcher–Goldfarb–Shanno (BFGS) minimization procedure [16,22]. In the outer region II, which extends theoretically to infinity, the larger distance from the defect allows the treatment of ionic relaxation by using the quasi-continuum procedures of the Mott–Littleton approximation [23]. To ensure a smooth transition between regions I and II, we incorporate an interfacial region, IIa, in which ion displacements are determined via the Mott–Littleton approximation, but in which interactions with ions in region I are calculated by explicit summation. For this kind of treatment of defects, it is crucial that proper convergence of the defect energies upon increasing the size of region I is achieved. In the present calculations, the radii of regions I and IIa were 10 and 30 Å, respectively.

In all calculations, we assume the volume of the supercell to be constant and equal to the calculated volume of bulk ceria ($a=b=c=5.469$ Å) due to the low defect concentration addressed. This assumption was justified by [14] showing that volume relaxation only has a minor effect on the defect parameters.

Although our calculations are for zero temperature, i.e., the lattice vibration entropy contributions are not included in the model, they allow us to uncover the generic energetic tendencies that exist in this system. The above computational methods are implemented in the GULP code [16], which was used throughout this work.

3. Results and discussion

There are two types of association energy definitions reported in the atomistic calculations. One is the difference between the formation energy of a defect cluster and the sum of the formation energies of the defect cluster's constituting point defects [10,25,26]. Another is the energy difference between a supercell and the supercell with the maximum energy [14,27]. Here, the latter definition was adopted on the basis of the following understanding.

At sufficiently high temperatures, the vacancy hopping is so fast that the existence of defect structures with high energy is possible. When ionic conduction occurs, the defect structure prefers to be the one with high energy in order to reduce the height of activation barrier for vacancy diffusion, that is, to make vacancy diffusion easier (as shown in Fig. 2(a)). On the contrary, the vacancy hopping greatly slows down at sufficiently low temperatures, which greatly reduces the possibility of the existence of defect structures with high energy. The defect structure at low temperature prefers to be the one with the lowest energy, that is, the thermodynamically most stable defect structure. Therefore, the activation barrier for vacancy diffusion at rather low temperature increases evidently compared to that at sufficiently high temperature. The energy difference between the two activation barriers could be defined as the association energy related to the ionic conductivity (as shown in Fig. 2(b)). The above definition of association energy provides us with a fairly clear physical picture associated with the ionic conductivity that is directly related to the vacancy diffusion in doped ceria.

Fig. 3 shows the association energies of ceria doped with different trivalent cations. For each given dopant cation, a more negative association energy results in a lower total energy and consequently the corresponding defect structure is more stable. First of all, we pay all attention to the association energies of the 1_1_1 and 1_1_2 defect structures (blue–black line and the pink line in Fig. 3). The association energies for the 1_1_1 defect structure decrease almost monotonously, and those for the 1_1_2 defect structure increase with the size of dopant cation. The crossover occurs at the position between Sm^{3+} and Nd^{3+} (that is, Pm^{3+}). The above trends are excellently consistent with recent first principle calculations [14] where the association energies for the above two defect structures are calculated. This virtually identical trend fully demonstrates and validates the utility of our calculations. The excellent agreement between our semi-empirical study and the first-principles study might be unexpected for such a highly complex mixed ionic–covalent system. As discussed in [27], the possible explanation comes from the fact that the relative association energy between different trivalent doped ceria is largely governed by the elastic interactions, which are easier to capture in model descriptions than complex electronic interactions. Further, if we consider all the possible defect structures, the energetic trends are somewhat different from the first principle calculations [14].

Now we consider all the possible defect structures in the 2×2×2 supercell and pay attention to the maximum association effect for different dopant cations. We then focus on the following matters: 1) the defect structure(s) with the lowest energy for different dopant cations, 2) the preferred vacancy–dopant separation and 3) the association energy trend with the dopant size. As shown in Fig. 3, the maximum association effects occur in the 1_1_1 defect structure for dopant cations smaller than Gd^{3+} and in the 3_2_2 defect structure for dopant cations larger than Gd^{3+}.

For dopant cations smaller than Gd^{3+}, the 1_1_1 defect structure is thermodynamically most stable. This implies that the vacancy prefers to associate with the dopant cations if the dopant cations are smaller than Gd^{3+}, while the dopant cation prefers to be in the nearest neighbor coordination cation shell around another dopant cation. This trend is excellently consistent with a recent extended X-ray absorption fine structure (EXAFS) investigation of 5 mol% Y^{3+} doped ceria [28], where it was found that Y^{3+} had a strong tendency to form an association with an oxygen vacancy and the Y^{3+} had a strong tendency to get together.

For dopant cations larger than Gd^{3+}, the association energies for the 3_2_2 and 4_2_2 defect structures are very close. No matter what defect structure forms, the two defect structures both mean that the

Table 3
Shell model parameters for O^{2-} and Ce^{4+}

Species	Charge (e)	K (eV Å^{-2})	Reference
O^{2-} core	0.04	6.3	23
O^{2-} shell	−2.04		
Ce^{4+} core	4.2	177.84	24
Ce^{4+} shell	−0.2		

*All dopant cations were treated as rigid ions.

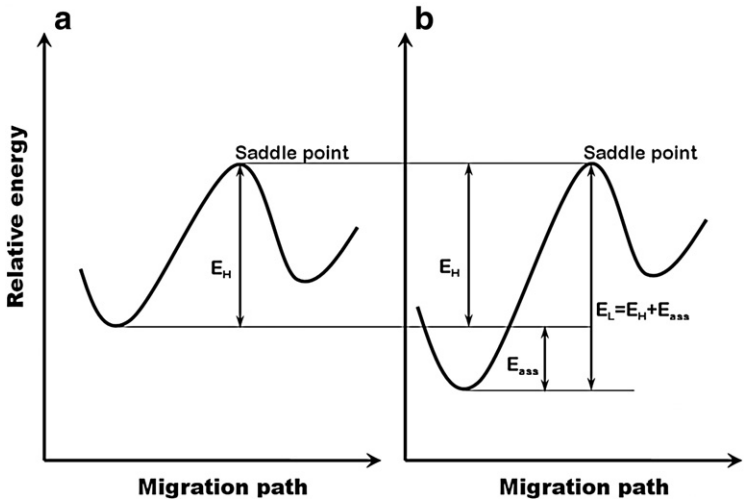

Fig. 2. Schematic illustration of the association energy related to the ionic conductivity of doped ceria at (a) higher temperature and (b) lower temperature. E_L is the diffusion barrier at low temperature and E_H is the diffusion barrier at high temperature. E_{ass} is the association energy.

vacancy energetically prefers to be in the second nearest coordination anion shell around the two dopant cations. This implies that the vacancy–Ce^{4+} association is preferable for the large dopant cations. Although this trend is not consistent with the EXAFS investigation for 5 mol% La^{3+} doped ceria where the same trend as for Y^{3+} doped ceria was presented [28], the trend that the large dopant cations prefer second neighbour sites was reported in a semi-empirical calculation of selected defect structures for doped ceria [10]. Moreover, our calculation results were also corroborated by the first principle and semi-empirical calculations for a stabilized cubic zirconia doped with trivalent cations [25–27] where it was shown that vacancies actually preferred to associate with the host ions (Zr^{4+}), rather than with dopant cations with a larger radius. In theory, the reasons for the vacancies' preference for the second neighbor sites of larger dopant cations in the fluorite structure (i.e., cubic stabilized zirconia and doped ceria) have been expatiated from two competing aspects [10,24,26], that is, lattice relaxation and coulomb interaction. The balance between relaxation and coulomb terms determines this site preference.

It is clear from Fig. 3 that the crossover of the maximum association energy occurs exactly at Gd^{3+}, which means that the vacancy–Gd^{3+} association is the weakest in trivalent doped ceria. Another interesting phenomenon is that the association energies for the 1_1_1, 3_1_2, 3_2_2 and 4_2_2 defect structures in the Gd^{3+} doped CeO_2 are extremely close. This indicates that the vacancy is unlikely to become bound to a cation at any particular coordination shell and a dopant cation is unlikely to become bound to another dopant cation at any particular coordination shell because for the above four defect structures, there is no particular vacancy–dopant and dopant–dopant arrangement that is preferred over another. This trend is fairly consistent with the EXAFS investigation of 5 mol% Gd^{3+} doped ceria where it is reported that Gd^{3+} is distributed randomly in the ceria lattice [28].

4. Conclusion

A clear preference for vacancy–dopant association occurs for small dopant cations and vacancy–Ce^{4+} association for large dopant cations,

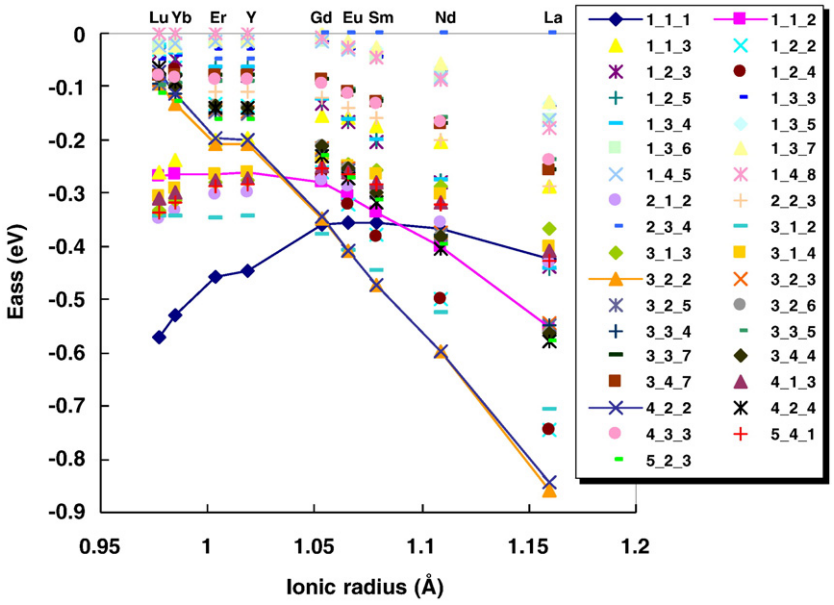

Fig. 3. Vacancy–dopant association energies (eV per vacancy) of different defect structures in ceria doped with 6.25 mol% trivalent cation. The lines are a guide for the eyes. (For interpretation of the references to colour in this figure legend, the reader is referred to the web version of this article.)

with the crossover exactly at Gd^{3+}. The maximum association effects occur in the 1_1_1 defect structure for dopant cations smaller than Gd^{3+} and in the 3_2_2 defect structure for dopant cations larger than Gd^{3+}. For Gd^{3+} doped ceria, which presents the lowest association effect in trivalent doped ceria, the association energies for the 1_1_1, 3_1_2, 3_2_2 and 4_2_2 defect structures are extremely close, which agrees well with a recent EXAFS investigation [28], that is, Gd^{3+} is distributed randomly in the ceria lattice.

Acknowledgements

The authors acknowledge support from the National Natural Science Foundation of China (Grants 50232020 and 50572042). We thank the High Performance Computing Center of Northwestern Polytechnical University for providing the calculation environments.

References

[1] B.C.H. Steele, A. Heinzel, Nature 414 (2001) 345.
[2] S. Park, J.M. Vohs, R.J. Gorte, Nature 404 (2000) 265.
[3] T. Hibino, A. Hashimoto, T. Inoue, J. Tokuno, S. Yoshida, M. Sano, Science 288 (2000) 2031.
[4] H. Inaba, H. Tagawa, Solid State Ion. 83 (1996) 1.
[5] M. Mogensen, N.M. Sammes, G.A. Tompsett, Solid State Ion. 129 (2000) 63.
[6] K. Huang, M. Feng, J.B. Goodenough, J. Am. Ceram. Soc. 81 (1998) 357.
[7] J.A. Kilner, R.J. Brook, Solid State Ion. 6 (1982) 237.
[8] X. Guo, R. Waser, Prog. Mater. Sci. 51 (2006) 151.
[9] V. Butler, C.R.A. Catlow, B.E.F. Fender, J.H. Harding, Solid State Ion. 8 (1983) 109.
[10] L. Minervini, M.O. Zacate, R.W. Grimes, Solid State Ion. 116 (1999) 339.
[11] G. Balducci, M.S. Islam, J. Kaspar, P. Fornasiero, M. Graziani, Chem. Mater. 15 (2003) 3781.
[12] J.A. Ball, R.W. Grimes, D.W. Price, Model. Simul. Mater. Sci. Eng. 13 (2005) 1353.
[13] H. Yoshid, T. Inagaki, K. Miura, M. Inaba, Z. Ogumi, Solid State Ion. 160 (2003) 109.
[14] D.A. Andersson, S.I. Simak, N.V. Skorodumova, I.A. Abrikosov, B. Johansson, Proc. Natl. Acad. Sci. U. S. A. 103 (2006) 3518.
[15] C.R.A. Catlow, R.G. Bell, J.D. Gale, J. Mater. Chem. 4 (1994) 781.
[16] J.D. Gale, A.L. Rohl, Mol. Sim. 29 (2003) 291.
[17] P.P. Ewald, Ann. Phys. (Leipzig) 64 (1921) 253.
[18] L. Minervini, R.W. Grimes, K.E. Sickafus, J. Am. Ceram. Soc. 83 (2000) 1873.
[19] R.W. Grimes, G. Busker, M.A. McCoy, A. Chroneos, J.A. Kilner, Ber. Bunsen-Ges. Phys. Chem. 101 (1997) 1204.
[20] S. Vyas, R.W. Grimes, D.H. Gay, A.L. Rohl, J. Chem. Soc., Faraday. Trans. 94 (1998) 427.
[21] B.G. Dick, A.W. Overhauser, Phys. Rev. 112 (1958) 90.
[22] D.F. Shanno, Math. Comput. 24 (1970) 647.
[23] N.F. Mott, M.J. Littleton, Trans. Faraday. Soc. 34 (1932) 485.
[24] A. Bogicevic, C. Wolverton, Phys. Rev. B 67 (2003) 024106.
[25] M.S. Khan, M.S. Islam, D.R. Bates, J. Mater. Chem. 8 (1998) 2299.
[26] M.O. Zacate, L. Minervini, D.J. Bradfield, R.W. Grimes, K.E. Sickafus, Solid State Ion. 128 (2000) 243.
[27] A. Bogicevic, C. Wolverton, G.M. Crosbie, E.B. Stechel, Phys. Rev. B 64 (2001) 014106.
[28] H. Deguchi, H. Yoshida, T. Inagaki, M. Horiuchi, Solid State Ion. 176 (2005) 1817.